RSC Advances

ROYAL SOCIETY OF CHEMISTRY

www.rsc.org/advances

GRAPHIC ABSTRACT

Hydrothermal in situ decomposition of DMF generated three $[NH_2(CH_3)_2]^+$ templated anionic zinc and cadmium terphenyl−3,2′,5′,3′′−tetracarboxyate frameworks, which show tunable luminescence in the presence of metal ions. Especially, **1** could be a luminescent sensor for selectively detecting traces of Ca^{2+} ions at ppm level in pyridine suspension.

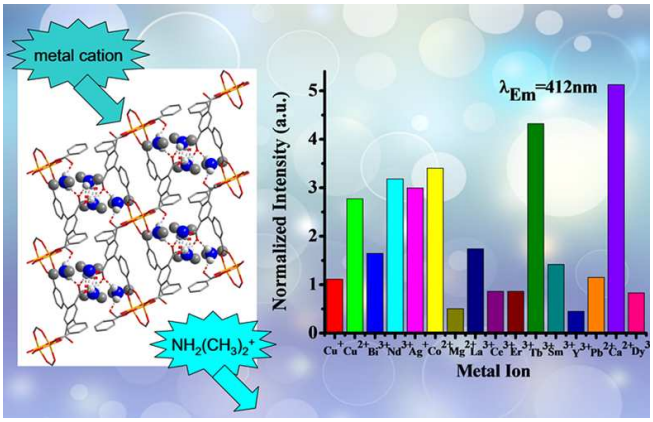

Journal Name

RSCPublishing

ARTICLE

Luminescent Group 12 Metal Tetracarboxylate Networks for Probe Metal Ions

Cite this: DOI: 10.1039/x0xx00000x

Hai-Yun Ren,[a] Cai-Yun Han, [a] Mei Qu [a] and Xian-Ming Zhang *[a]

Received 00th January 2012,
Accepted 00th January 2012

DOI: 10.1039/x0xx00000x

www.rsc.org/

Hydrothermal in situ decomposition of DMF generated three $[NH_2(CH_3)_2]^+$ cation templated anionic zinc and cadmium terphenyl-3,2′,5′,3′-tetracarboxyate (tpta) frameworks. Compound **1** shows *kgd* topological layer constructed by 6-connected paddlewheel-type $[Zn_2(CO_2)_4]$ SUBs and 3-connected tpta groups. Compound **2** has 3D *sra* network constructed by zigzag chains of metal centers and tpta groups. Compound **3** adopts a new (4,7)-connected topological network with four kinds of nodes. Compounds **1**−**3** show two blue phosphorescent emission bands attributed to ligand centered transitions perturbed by metal ions, which displays significant temperature-dependent behavior. The higher energy emissions are red-shift and weakened with increase of temperature while the lower energy emissions increase in intensity and finally become to main emission bands; the CIE coordinates for **1** are changed with lowing of temperature from blue to greenish blue. Interestingly, **1** could selectively detect traces of Ca^{2+} ions at ppm level in pyridine suspension, which make it more suitable as luminescent probes for sensing Ca^{+} ions.

Introduction

Postsynthetic modification of metal-organic frameworks (MOFs) via diffusion or exchange of atoms has recently been attracting the current interest of the material scientists, because it can be a simple and versatile way to modify the physical environment of the pores and cavities within MOFs which can be utilized for gas storage, molecular sensors, nonlinear optical devices, and so on.[1] For instance, a reversible switch of the inversion symmetry in a cobalt ferrocyanide framework was achieved by alkaline cation exchange, which can effectively control the second harmonic generation activity of compound $K_{1.88}Co[Fe(CN)_6]C_{0.97}$ at room temperature.[2] However, cation-exchange within anionic MOFs, in particular, has been shown to be very easy to modify physical properties of the host framework.[3] By cation exchange procedures, luminescent anionic MOFs have been proven successful in the detection of volatile organic compounds, small molecules, and ionic species. Synthetically, the rational design in construction of anionic metal−carboxylate frameworks may borrow organic template idea from traditional aluminosilicates.[4] By using N,N′−dimethylformamide (DMF) as precursors of $[NH_2(CH_3)_2]^+$ templates, Sun et al prepared an anion luminescent europium–tetracarboxylates which could selectively sense Fe^{3+} and Al^{3+} ions through fluorescence quenching and enhancement, respectively.[5] Recently, transition-metal-based luminescent MOFs have been focused on d^{10} zinc and cadmium MOFs because these metal ions not only possess various coordination numbers and geometries, but also exhibit superior luminescent properties when bound to functional ligands, which make them particularly suitable for the development of optical devices and tunable luminescent sensors for chemical species.[6] To be note, anionic zinc and cadmium tetracarboxylate frameworks with tunable luminescent properties for probe metal ions are still rare.

In the ongoing research of porous luminescent frameworks, multifunctional terphenyl−3, 2′, 5′, 3′−tetracarboxylic acid (H_4tpta) attracted our attention. First, H_4tpta can be twisted by different degrees across the C–C single bonds, possessing both rigidity and flexibility. Second, it has significant degree of conjugation which often induces strong absorption and emission. Additionally, the electron-withdrawing carboxylic groups of H_4tpta can enhance probability of the intersystem crossing from the first excited singlet state to the triplet state, to promote the emission of phosphorescence.[7]

In this paper, by in situ hydrolysis of DMF to generate $[NH_2(CH_3)_2]^+$ cations, we present herein the syntheses, structures, and luminescent properties of three anion open frameworks $[Me_2NH_2]_2[Zn(tpta)]$ (**1**), $[Me_2NH_2]_2[Cd(tpta)]\cdot H_2O$ (**2**), and $[Me_2NH_2]_3[Cd_{2.5}(tpta)(H_2O)(DMF)_{0.5}]\cdot 3DMF$ (**3**), along with their optical response to the exchange of cationic guest molecules. The comparison of photoluminescent spectra for free H_4tpta and **1**−**3** suggest coordination of tpta ligands to metal clusters could impose structural rigidity and slightly tune its electronic structure, leading to red shift of emission and long lifetime. The emission spectra of **1**−**3** all show strong temperature-dependence. From 4K to 298 K, the centered emission is inversed between the higher energy band and the lower band in **1**−**3**. Compound **1** in a pyridine suspension exhibits high sensitivity for detection of Ca^{2+}, which show that it may be efficient phosphorescence sensor.

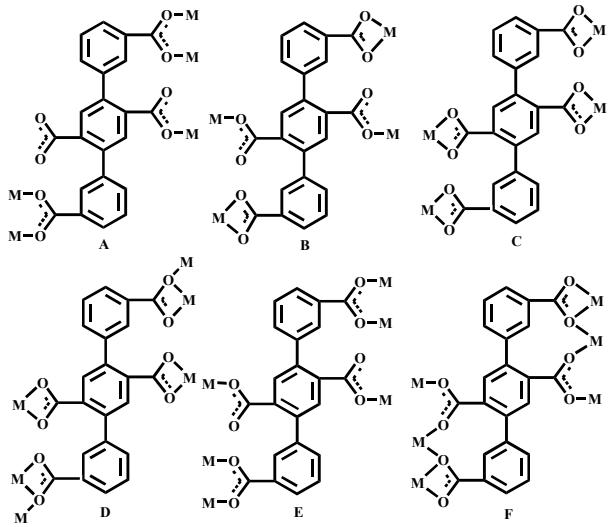

Scheme. 1 Schematic view of coordination modes of tpta ligands.

Experimental

Materials and Methods

All chemicals were analytically pure from commercial sources and used without further purification. Elemental analyses were performed on a Vario EL-II analyzer. FTIR spectra were recorded from KBr pellets in the range 4000−400 cm^{-1} on a Perkin-Elmer Spectrum BX FT-IR spectrometer. Variable temperature powder X-ray diffraction (VT-PXRD) data were collected in a Bruker D8 advance diffractometerusing Cu Kα radiation.. The purity of all compounds was confirmed by comparison of experimental PXRD patterns with the simulated pattern derived from the X-ray single crystal data compound. Photoluminescence was performed on an Edinburgh FLS920 luminescence spectrometer. The luminescent quantum yields of **1**−**3** were measured using an absolute method[8] by calibrated integrating sphere. The low temperature luminescence was performed on a Janis SHI-4s-1 closed cycle refrigerator, which provides a convenient means of cooling samples to temperatures 4K by a closed loop of helium gas. The thermogravimetric analyses (TGA) were carried out in air atmosphere using SETARAM LABSYS equipment at a heating rate of 10 °C/min.

X-ray Crystallography.

X-ray single-crystal diffraction data for **1**−**3** were collected on a Bruker Smart APEX CCD diffractometer at 298(2) K using Mo Kα radiation (λ = 0.71073 Å). The program SAINT was used for integration of the diffraction profiles, and the program SADABS was used for absorption correction. All the structures were solved by direct method using the SHELXS program of the SHELXTL package and refined by full-matrix least-squares technique with SHELXL.[9] All non-hydrogen atoms were refined with anisotropic thermal parameters. Hydrogen atoms of organic ligand were generated theoretically onto the specific carbon and refined isotropically with fixed thermal factors. Further details for structural analysis are summarized in Table 1 and selected bond lengths and angles are shown in the Supporting Information.

Syntheses.

Tab. 1 Crystallographic Data and Structure Refinement for **1**−**3**

Compound	1	2	3
Formula	$C_{26}H_{21}ZnN_2O_8$	$C_{26}H_{28}CdN_2O_9$	$C_{47.5}H_{32.5}Cd_{2.5}N_{1.5}O_{17.5}$
Fw	559.86	624.91	1185.25
Crystal system	Triclinic	Monoclinic	Triclinic
Space group	P-1	P21/c	P-1
a (Å)	9.5418(4)	13.5667(10)	11.2195(4)
b (Å)	11.2720(8)	9.5666(8)	15.8170(7)
c (Å)	12.7837(7)	23.1432(13)	18.0989(6)
α (°)	112.512(6)	90	102.099(3)
β (°)	90.364(4)	122.672(6)	96.385(3)
γ (°)	91.241(5)	90	98.947(3)
V (Å^3)	1269.72(12)	2528.4(3)	3067.7(2)
Z	2	4	2
ρ_{calc} (g cm^{-3})	1.464	1.642	1.283
F(000)	580	1272	1176
Reflections	9378 / 5337	11230 / 5155	22875/12518
Data/ parameters	5337 / 398	5155/ 351	12518/653
S	1.004	1.045	1.035
R_1[a]	0.0381	0.0413	0.0498
wR_2[b]	0.0825	0.1087	0.1521
$\Delta\rho_{max}/\Delta\rho_{min}$(eA^{-3})	0.363/-0.408	1.635/-1.501	1.731/-0.771

[a] $R_1 = \sum||F_o|-|F_c||/\sum|F_o|$. [b] $wR_2 = [\sum[w(F_o^2-F_c^2)^2]/\sum[w(F_o^2)^2]]^{1/2}$

$[Me_2NH_2]_2[Zn(tpta)]$ (**1**). A mixture of $ZnCl_2$ (0.056 g, 0.40 mmol), H_4tpta (0.042 g, 0.10 mmol), $NH_3\cdot H_2O$ (0.1 ml/5M, 0.5 mmol), DMF (3 ml) was stirred, then sealed in a 15 mL Teflon-lined stainless autoclave at 150 °C for 6 days. After it was cooled to room temperature and subjected to filtration, yellow block crystals of **1** in yield of 68.6% (based on H_4tpta) were recovered. Anal. Calcd (%) for $C_{26}H_{21}ZnN_2O_8$ (**1**): C, 56.28; H, 3.78; N, 5.05. Found: C, 55.82; H, 3.69; N, 4.95. IR data (KBr, cm^{-1}): 3454(b), 2354(w), 1626(s), 1482(s), 1098(w), 843(w), 796(s).

$[Me_2NH_2]_2[Cd(tpta)]\cdot H_2O$ (**2**). A mixture of $CdBr_2$ (0.104 g, 0.3 mmol), H_4tpta (0.041 g, 0.1 mmol), $NH_3\cdot H_2O$ (0.1 ml/5M, 0.5 mmol), DMF (3 ml) was stirred, then sealed in a 15 mL Teflon-lined stainless autoclave at 130 °C for 6 days. After it was cooled to room temperature and subjected to filtration, yellow block crystals of **2** in yield of 56.7% (based on H_4tpta) were recovered. Anal. Calcd (%) for $C_{26}H_{28}CdN_2O_9$ (**2**): C, 49.97; H, 4.52; N, 4.48. Found: C, 50.11; H, 4.42; N, 4.73. IR data (KBr, cm^{-1}): 3424(b), 2344(w), 1616(s), 1400(vs), 998(w), 832(w), 598(w).

$[Me_2NH_2]_3[Cd_{2.5}(tpta)_2(H_2O)(DMF)_{0.5}]\cdot 3DMF$ (**3**). A mixture of $CdBr_2$ (0.138 g, 0.4 mmol), H_4tpta (0.041 g, 0.1 mmol), $NH_3\cdot H_2O$ (0.1 ml/5M, 0.5 mmol), DMF (3 ml) was stirred, then sealed in a 15 mL Teflon-lined stainless autoclave at 130 °C for 6 days. After it was cooled to room temperature and subjected to filtration, yellow block crystals of **3** in yield of 86.7% (based on H_4tpta) were recovered. Anal. Calcd (%) for $C_{60}H_{70.5}Cd_{2.5}N_{6.5}O_{20.5}$ (**3**): C, 48.31; H, 4.76; N, 6.10. Found: C, 49.63; H, 4.62; N, 6.03. IR data (KBr, cm^{-1}): 3452(b), 2352(w), 1570(s), 1368(vs), 826(w), 760(w), 588(w).

Preparation of Suspension.

First, finely grinded 2 mg samples of **1**, **2** and **3** were immersed in different organic solvents (4 mL), treated by ultrasonication for 1 h, and then sealed in 5 mL vials to age for 3 days to form stable suspensions before luminescence study.

Second, **1** was immersed in pyridine containing equivalent nitrate { $M(NO_3)_x$, M = Mg^{2+}, Ca^{2+}, Co^{2+}, Cu^{+}, Cu^{2+}, Ag^{+}, Pb^{2+}, Bi^{3+}, Nd^{3+}, Dy^{3+}, La^{3+}, Ce^{3+}, Er^{3+}, Tb^{3+}, Sm^{3+}, Y^{3+}}, **2** and **3** was immersed in 1,2,4−trichlorobenzene containing equivalent nitrate {$M(NO_3)_x$, M = Ca^{2+}, Cu^{+}, Cu^{2+}, Ag^{+}, Nd^{3+}, Dy^{3+}, Ce^{3+}, Er^{3+}, Tb^{3+}, Sm^{3+}, Y^{3+}, Eu^{3+}, La^{3+}, Gd^{3+}, Bi^{3+}}, treated by ultrasonication for 1 h, and then sealed in 5 mL vials at 85 °C for 3 days to perform cation-exchange for luminescence studies. Third, **1** was immersed in pyridine containing different concentration of $Ca(NO_3)_2$ treated by ultrasonication for 1 h, and then sealed in 5 mL vials at 85 °C for 3 days to perform cation-exchange for luminescence studies.

Results and discussion

Description of Structures

Compound **1** crystallizes in the triclinic space group *P-1* with an asymmetric unit consisting of one crystallographically independent Zn(II) ions, one tpta, and two $[Me_2NH_2]^+$ cations as shown in Fig. S1. The dihedral angle of the two phenyls of tpta is 146.69°, in agreement with semirigid nature of tpta. The Zn(1) resides in a distorted square pyramidal geometry, ligated by four bis(monodentate) carboxylate oxygen atoms in the equatorial plane and one monodentate carboxylate oxygen atom at the axial position. The slightly distorted square pyramidal environment is evidenced by the discrimination parameter (τ) value 0.001, defined as $|\beta-\alpha|/60$ by Addison et al.[10] The carboxylate O(3)−C−O(4) is also deprotonated as a result of formation N–H···O hydrogen bond with $[Me_2NH_2]^+$ cations. The Zn−O distances in the equatorial plane are in the range of 2.028(2) −2.072 (2) Å, and the axial shorter Zn(1)−O(1) distance is 1.971(2) Å. The coordination bond angles around Zn(II) vary from 86.37(8)° to 157.50(7)°. The ligand tpta adopt μ_5-coordination mode: two carboxylate groups in μ_2–η^1:η^1–bridging modes are connected two Zn(II) atoms with a Zn···Zn separations of 3.0268(5) Å, whereas other carboxylate groups are coordinated in monodentate mode (Scheme 1, A). In **1**, Zn(1) atoms are bridged by four carboxylates to generate paddlewheel-type $[Zn_2(COO)_4]$ SUBs, each of which is surrounded by six tpta groups. Meanwhile, each tpta can link three SUBs to yield a 2D layer (Fig. S2). Topological analysis revealed that the 2D layer exhibits a planar *kgd* net with a short *Schläfli* symbol $[4^3]_2[4^6.6^6.8^3]$, in which $[Zn_2(COO)_4]$ SBUs act as 6-connected nodes and tpta groups act as the 3-connected nodes (Fig. S3). The $[Me_2NH_2]^+$ cations in situ generated by the decomposition of DMF molecules are filled between adjacent layers via N–H···O hydrogen bonds (Fig. 1).

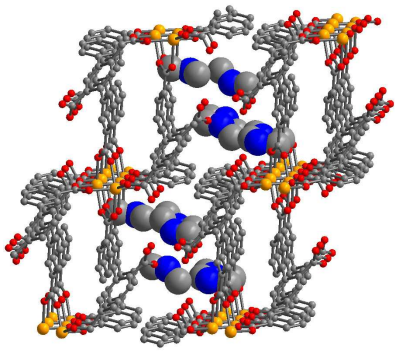

Fig. 1 View of packing two layers showing interlayer $[Me_2NH_2]^+$ cation.

Compound **2** crystallizes in the monoclinic space group $P2_1/c$. The asymmetric unit consists of one crystallographically independent Cd(II) ion, one tpta, two $[Me_2NH_2]^+$ cations, and one water molecule as shown in Fig. S4. Compared with **1**, the smaller torsion angle of the two phenyls of tpta is 134.3°. Cd(II) displays a distorted octahedral geometry, coordinated by eight carboxylate oxygen atoms from four tpta groups. The Cd(1)−O distances are from 2.236(4) to 2.448(4) Å in the equatorial plane and 2.277(4) to 2.370(5) Å in the axial positions. The O−Cd(1)−O bond angles are in the range of 54.08(15)° and 170.36(17)°. The tpta group shows μ_4-mode (Scheme 1, B). **2** has a 3D microporous *sra* topological net with short *Schläfli* symbol $[4^2.6^3.8]$, possessing two different four-connected nodes (Fig. S5).[11] The calculated void volume is 736 $Å^3$ per unit cell, which is filled by water molecules and $[Me_2NH_2]^+$ cations. The $[Me_2NH_2]^+$ cations play an important role in charge-compensation and space-filling As shown in Fig. 2, the channel window is closed, which suggests the encapsulated $[Me_2NH_2]^+$ cations could not be facilely exchanged.

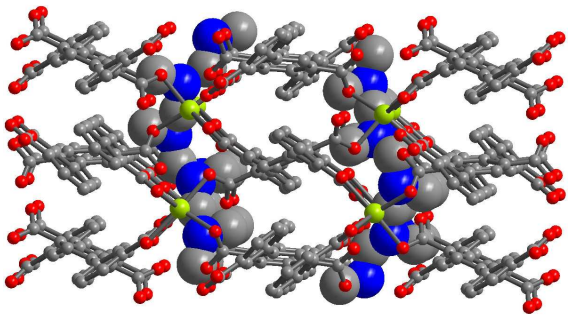

Fig. 2 View of 3D framework of **2** along the *a*-axis direction showing $[Me_2NH_2]^+$ cations encapsulated. Hydrogen bonds are represented by dashed lines.

Compound **3** crystallizes in triclinic space group P-*1* and the asymmetric unit consists of three Cd(II) ions, two tpta, and one $[Me_2NH_2]^+$ cation. Charge balance and thermal gravimetric analyses indicate that there are non-located $[Me_2NH_2]^+$ cations, which is normally observed in porous MOFs. As shown in Fig. S6, the Cd(1) ions coordinated with seven oxygen atoms to form a distorted capped octahedron. The Cd(1)–O bond lengths vary in the large range of 2.196(8)–2.826(6) Å and corresponding O−Cd(1)−O range from 53.4(2)° to 167.4(4)°.[12] The Cd(2) site adopts an octahedral coordination geometry ligated by four O atoms from four different tpta, one terminal water molecules, and one O atom from DMF. The Cd(2) localizes special positions with site occupancy of 0.5. The Cd(2)–O bond lengths are within the range of 2.070(15)–2.407(7) Å. The *cis*- and *trans*-O−Cd(2)−O angles are in the range of 81.9(2)°-98.4(3)° and 173.1(2)°-176.4(4)°, respectively. Cd(3) atom is occupied by six O atoms from four individual tpta in an highly distorted octahedral geometry. The Cd(3)–O bond lengths are in the range 2.184(8)–2.401(7) Å. The *cis*- and *trans*-O−Cd(3)−O are in the range of 54.6(2)-111.7(3)° and 152.4(2)-165.4(3)°, respectively, indicating highly distortion from an octahedral coordination geometry. Compared with **1** and **2**, tpta ligands in **3** adopt one μ_4– and three different μ_6–coordination modes as shown in C, D, E and F in Scheme 1. Two carboxylate groups adopt μ_2–η^1: η^2–chelating–bidentate and μ_2–η^1: η^1–syn–syn–bidentate modes to connect two shared-vertex Cd atoms with Cd···Cd distances of 3.9812(12) and 4.1153(14) Å. **3** adopts a new (4,7)-connected topological network with the *Schläfli* symbol $[4^2.5^2.7^2][4^4.5.6][4^4.6^2][4^9.5^3.6^9]_2$. It is interesting that there are four kinds of nodes. As shown in Fig. S7, vertex-sharing Cd(1)–Cd(2)–Cd(3) trimers act as 7-connected nodes, and the tpta ligands in Scheme 1C, D and E act as different 4-connected nodes, but the tpta ligands in Scheme 1F act as linkers.

The calculated void volume is 971.3 Å^3 per unit cell, namely 31.7%, which is filled by $[Me_2NH_2]^+$ cations and DMF molecules. The organic cations $[Me_2NH_2]^+$ for charge-compensation and space-filling are fixed via N–H···O hydrogen bonds in the channels and holes. The channel window is closed, which indicates that the encapsulated $[Me_2NH_2]^+$ cations may not be easily exchanged (Fig. 3).

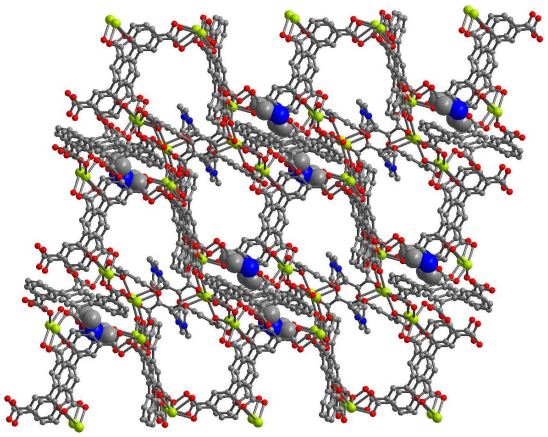

Fig. 3 View of the 3D framework of **3** along the *a*-axis direction showing $[Me_2NH_2]^+$ cation encapsulated.

Photoluminescence and sensing.

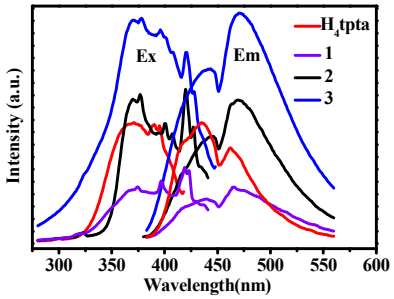

Fig. 4 Solid-state emission and excitation spectra of **1-3** as well as free H_4tpta.

As shown in Fig. 5a, the room temperature photoluminescence spectra of **1**−**3** as well as free ligand H_4tpta in solid state have been investigated (Fig. 4). H_4tpta show broad luminescence upon excitation at 367 nm, with a central peak at 435 nm and a low energy peak at 462 nm, which can be assigned to π*→*n* and π*→π transitions.[13] The lifetime of the main emission band for H_4tpta is 27.19 *μ*s. Compared with free H_4tpta, both the low and high energy peaks in **1**−**3** are red-shifted about 4–11 nm (Tab. S6). What is more important is that relative intensities of the low and high energy peaks are inversed, the low energy peaks become to the main emission bands. The luminescent quantum yield for **1**−**3** was determined by means of an integrating sphere and was found to be 31.05%, 36.42%, 39.81%, respectively. The lifetime of the main emission bands for **1**−**3** were increased to 44.70, 64.63, 73.33 *μ*s, respectively, suggesting some character of phosphorescence. Emissions of **1**−**3** are very similar to the free ligand, which may be mainly ligand-centered electronic transitions perturbed by metal ions.[14] In this case, the red-shifted phenomenon and increase of lifetime for **1**−**3** may possibly be attributed to the increased stability of ligands within **1**−**3**. In addition, coordination environment of metal ions could affect orientation of organic ligands which results in the difference in emissions in **1**−**3**.

The variable temperature luminescence spectra of **1**−**3** from 4 K to 298 K are shown in Fig. 5a. The luminescence maxima and intensities of **1**−**3** showed temperature-dependent[15]. At 4 K, the emission spectrum of **1** displays a higher energy peak centered at λ_{max} = 420 nm, and a lower energy peak at about 467 nm (Fig. 5a). The peak at higher energy undergoes a red shift to 430 nm at 100 K, 439 nm at 200 K, 443 nm at 298 K (Tab. S6), but reduces in intensity.[16] Although the maximum of the lower energy peak makes no move, the intensity progressively increases from 4 K to 298 K. With raised temperatures, relative intensities of emissions bands at the lower and higher energy are inversed gradually. In the range of 4−200 K, the emission is dominated by a higher energy band, and the lower energy band is extremely weak while the luminescence is dominated by the lower energy one at room temperature. The inverse emission maxima observed herein suggest different mechanisms. Based on Commission International de L'Eclairage (CIE) chromaticity diagram, the corresponding CIE coordinates were calculated and the values are (0.1428, 0.1398), (0.1376, 0.1729), (0.1349, 0.1854), and (0.1355, 0.1875) for 4 K, 100 K, 200 K and 298 K, respectively (Fig. 5b). With increasing temperature, the chromaticity coordinates apparently changed from blue to greenish blue. As shown in Fig. S8a and S9a, the emission spectra of **2** and **3** display similar change with increased temperature: the higher energy emission peaks red-shift accompanied decreased intensity; the lower energy emission peaks increase significantly in intensity and finally become to the main emission bands; the chromaticity coordinates changed from blue to greenish blue from 4 K to 298K, which may be ascribed to decrease of chromophore aggregation with increased temperature (Fig. S8b −S9b). [14]

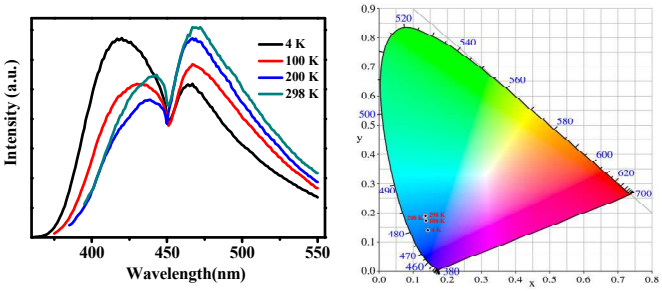

Fig. 5. (a) Emission spectra of **1** from 4 to 298K with λ_{ex}= 374 nm; (b) the CIE coordinates (marked by the circles) for **1** at various temperature

As mentioned above, $[Me_2NH_2]^+$ groups are located in the channels of the three anionic frameworks, which provided us a chance to study the ion-exchange and its effect on luminescence.[17] Taking into account important role of solvents, several experiments were then performed in different solvents to determine optimized solvent before cation-exchange. As shown in Fig. 6, the suspension of **1** in pyridine remarkably enhances the phosphorescence intensity of **1**, which may be due to extend π-system of tpta as linker and increase a significant degree of conjugation by hydrogen bond between pyridine with **1**. Its emission spectrum displays a central peak at 436 nm with additional peaks at higher energy of 414 nm and lower energy of 466 nm, slightly different from the maximum emission at 476 nm for free H_4tpta in pyridine. The difference in

their emissions is probably due that the reaction of proton of H_4tpta with nitrogen atom of pyridine could change the ratio of acid and conjugate base of H_4tpta (Fig. S10a). In contrast, other solvents such as water, alcohols (methanol, ethanol, isopropanol, *n*-butanol, and *n*-hexanol), acetone, amides, CH_2Cl_2 and actonitrile have a less effect on luminescence of **1.**

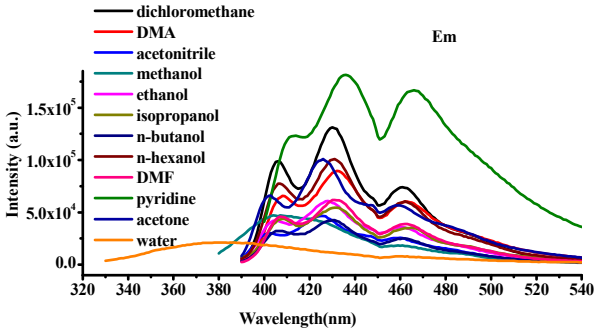

Fig. 6 Phosphorescence emissions of **1** in different solvents

With optimized solvent established, the phosphorescent enhancement effects of various metal ions on **1** in a pyridine suspension were investigated under excitation at 378 nm. After cation exchange as shown in Fig. 7, Ca^{2+} could remarkably increase luminescence intensity much more than other metal ions which may result from more effective intramolecular energy transfer.[18] As is well known, a highly selective probe for Ca^{2+} gives a positive response rather than phosphorescent quenching, which is usually preferred to promote sensitivity.

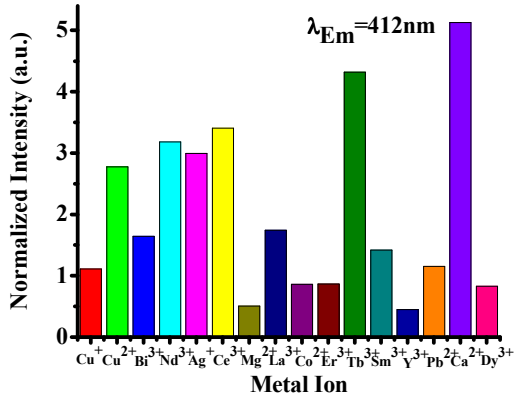

Fig. 7 Phosphorescence response of **1** to metal ions showing selectivity for Ca^{2+} in pyridine.

To further explore the availability of **1** as a highly selective probe for Ca^{2+}, phosphorescent spectra of **1** in different concentration of Ca^{2+} were examined (Fig. 8). Firstly, the highest concentration probed for Ca^{2+} was up to 16 mM. When increased the concentration of Ca^{2+} again, the phosphorescence intensity of **1** in a pyridine suspension had no significant spectral changes. Secondly, the lowest concentration was 1.3×10^{-3} mM. A good linear correlation (R^2=0.974) exists between phosphorescence efficiency and concentration of Ca^{2+} over the range of $1.3\times10^{-3} \sim 4\times10^{-3}$ mM in Fig. 9.

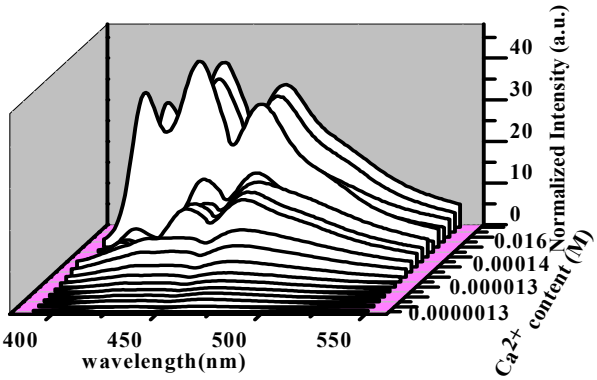

Fig. 8 The PL emission of **1** in the presence of various concentration of Ca^{2+} in pyridine**.**

As shown in Fig. S11, the suspension of **2** in 1,2,4−trichlorobenzene displays stronger emission with maximum peak at 440 nm with additional peaks at higher energy of 414 nm and lower energy of 468 nm than other solvents, which may be due to the fact that large spin-orbit coupling of halogen atoms induce heavy-atom effect to increase the intersystem crossing. [19] In contrast to **2**, the suspension of **3** in 1, 2, 4−trichlorobenzene also shows strongest emission with a little red-shift (Fig. S12). Both are similar with emissions of H_4tpta in 1,2,4−trichlorobenzene (Fig. S10b), which may be due to ligand-centered electronic transitions.

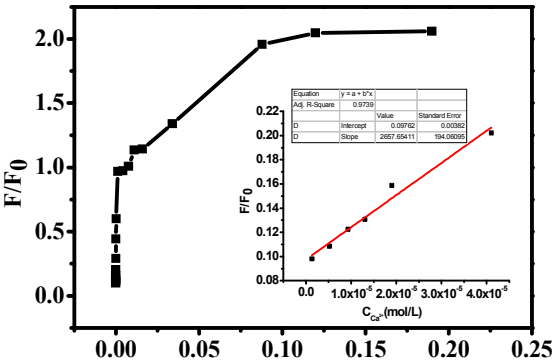

Fig. 9 Plot of the enhance efficiency of **1** dispersed in pyridine at different concentrations of Ca^{2+}. Emission intensities were selected at 414 nm. Inset: linear relation between the enhance efficiency and the concentrations of Ca^{2+} in the range of 1.3×10^{-3} ~16 mm.

The phosphorescent enhancement effects of various metal ions on **2** and **3** in 1,2,4−trichlorobenzene were then investigated under excitation at 380 nm. As shown in Fig. S13 and S14, after cations-exchange, most metal ions give positive response. However, compared with the suspension of **1** in pyridine, **2** and **3** in 1,2,4−trichlorobenzene exhibit poor selectivity. This phenomenon might be explained as follows: i) $[Me_2NH_2]^+$ cations were encapsulated in the closed channel window in **2** and **3**, and thus could not be efficiently exchanged. ii) 1,2,4-trichlorobenzene as solvent disturbs phosphorescence response of **2** and **3**.

Thermal Analyses.

The thermogravimetric analyses of polycrystalline samples of **1**–**3** were performed in air at a heating rate of 10 °C /min^{-1}. The thermal stability of **1**–**3** was further assessed by VT-XRPD. As shown in Fig. S15−18, different coordination networks of **1**–**3** result in different thermal stabilities. For **1**, as shown in the VT-XRPD (Fig. S16), the main network of compound **1** may be stable up to 250 °C, which illustrates good thermal stability. the

first weight loss of 59.2% in the temperature range of 260−520 °C is in agreement with the removal of $[Me_2NH_2]^+$ cations and partial tpta ligand, accompanied by the decomposition of the framework. The continuous loss arises upon further heating; a stable residue is not formed up to 1100 °C. For **2**, the framework remains intact up to 250 °C in the VT-XRPD (Fig. S17). However, as shown in Fig. 15, the weight loss begins at 180 °C. The continuous weight loss of 73.50% in the range of 190–580 °C corresponds to the removal of tpta ligand and $[Me_2NH_2]^+$ cations, which is followed by decomposition of framework. The final residue of 19.8% (*Calcd.* 20.5%) for **2** is closed to the percentage of CdO. For **3**, with increased temperature in Fig. 18, 2θ values of the corresponding diffraction peaks are slightly lower (~0.14°) than those of the one simulated at 298 K, implying that the crystal structure varies a little bit at different temperatures. The TG analysis display the first weight loss of 28.3% (*Calcd*. 27.5%) within the range 40–360 °C corresponds to the removal of one water, three DMF molecules and three $[Me_2NH_2]^+$ cations, which is followed by the decomposition of the framework. The final residue of 21.3% is in agreement with CdO (*Calcd*. 21.5%).

Conclusions

Hydrothermal in situ decomposition of DMF generated three $[NH_2(CH_3)_2]^+$ cation templated zinc and cadmium terphenyl-3,2′,5′, 3′-tetracarboxyate anionic frameworks. With increased temperature from 4 K to 298 K, emission spectra of **1**−**3** show temperature-dependent: emission maxima are gradually inversed from higher energy band to lower band. Correspondingly, CIE coordinates are changed from blue to greenish blue. Interestingly, the dispersed suspension of **1** in pyridine exhibits strong phosphoresce emission, which can selectively probe for traces of Ca^{2+} at ppm level. The selective probe indicates that $[Me_2NH_2]^+$ cations between the layers could be exhanged by Ca^{2+} ions, which have a significant effect on the phosphorescence intensity. The high selectivity and sensitivity of the phosphoresce response of **1** to metal ions shows what could be used as efficient phosphoresce sensor.

Acknowledgements

The acknowledgements This work was financially supported by the 973 Program (2012CB821701), the Ministry of Education of China (No. IRT1156), National Science Fund for Distinguished Young Scholars (20925101), and Shanxi Fund for Returned Oversea Scholars.

Notes and references

[a] School of Chemistry & Material Science, Shanxi Normal University, Linfen, Shanxi 041004 China

† Electronic Supplementary Information (ESI) available: [Figures showing structural details, IR, TG, XRPD and crystallographic cif data for **1**–**3**, emission spectra of **2**–**3** from and the CIE coordinates for **2**–**3** at various temperature, emission and excitation spectra of H_4tpta in pyridine and 1,2,4-trichlorobenzene, solid-state photoluminescence spectra, phosphorescence emission changes of **2**–**3** in different solvents, phosphorescence response of **2**–**3** to various cations have been included.]. See DOI: 10.1039/b000000x/

1 (a) J. An, N. L. Rosi, *J. Am. Chem. Soc.* 2010, **132**, 5578. (b) J. An, C. M. Shade, D. A. Chengelis-Czegan, S. Petoud, N. L. Rosi, *J. Am. Chem. Soc.* 2011, **133**, 1220. (c) S. Ganguly, P. Pachfule, S. Bala, A. Goswami, S. Bhattacharya, R. Mondal, *Inorg. Chem.* 2013, **52**, 3588. (d) Y. F. Han, G. X. Jin, F. E. Hahn, *J. Am. Chem. Soc.* 2013, **135**, 9263.(e) M. J. Ingleson, R. Heck, J. A. Gould, M. J. Rosseinsky, *Inorg. Chem.* 2009, **48**, 9986. (f) J. W. Shin, J. M. Bae, C. Kim, K. S. Min, *Inorg. Chem.* 2013, **52**, 2265. (g) S. C. Jones, C. A. Bauer, *J. Am. Chem. Soc.* 2009, **131**, 12516. (h) K. Miszta, D. Dorfs, A. Genovese, M. R. Kim, L. Manna, *ACS. Nano.* 2011, **5**, 7176. (i) D. J. Lun, G. I. N. Waterhouse, S. G. Telfer, *J. Am. Chem. Soc.* 2011, **133**, 5806. (j) M. Meilikhov, K. Yusenko, R. A. Fischer, *J. Am. Chem. Soc.* 2009, **131**, 9644. (k) J. G. Nguyen, S. M. Cohen, *J. Am. Chem. Soc.* 2010, **132**, 4560. (l) J. A. Thompson, N. A. Brunelli, R. P. Lively, J. R. C. W. Johnson, Jones, S. Nair, *J. Phys. Chem. C.* 2013, **117**, 8198. (m) Z. Wang, S. M. Cohen, *J. Am. Chem. Soc.* 2007, **129**, 12368. (n) Z. Wang, S. M. Cohen, *J. Am. Chem. Soc*. 2009, **131**, 16675.

2 (a) T. Matsuda, J. Kim, Y. Moritomo, *J. Am. Chem. Soc.* 2010, **132**, 12206. (b) V. Sazonova, Y. Yaish, H. Ustunel, D. Roundy, T. A. Arias, P. L. McEuen, *Nat.* 2004, **431**, 284.

3 W. G. Lu, L. Jiang, X. L. Feng, T. B. Lu, *Inorg. Chem.* 2009, **48**, 6997.

4 (a) A. K. Cheetham, G. Férey, T. Loiseau, *Angew. Chem. Int. Ed.* 1999, **38**, 3268. (b) A. Corma, F. Rey, J. Rius, M. J. Sabater, S. Valencia, *Nat.* 2004, **431**, 287.

5 Z. Chen, Y. W. Sun, L. L. Zhang, D. Sun, F. L. Liu, Q. G. Meng, R. M. Wang, D. F. Sun, *Chem. Commun.* 2013, **49**, 11557.

6 Y. Cui, Y. Yue, G. Qian, B. Chen, *Chem. Rev.* 2012, **112**, 1126.

7 A. Nollet, *Structural Effects on Fluorescence Emission: In Molecular Fluorcence*; B. Valeur, M. N. Berberan-Santos; Wiley-VCH: Weinheim, 2012, pp 75.

8 Y. Kawamura, H. Sasabe, C. Adachi. *Jpn. J. Appl. Phys., Part 1,* 2004, **43**, 7729.

9 G. M. Sheldrick, *SHELX-97*, *Program for X-ray Crystal Structure Solution and Refinement*; Göttingen University: Germany, 1997.

10 S. Majumder, L. Mandal, S. Mohanta, *Inorg. Chem.* 2012, **51**, 8739.

11 (a) L. N. Jia, L. Hou, L. Wei, X. J. Jing, B. Liu, Y. Y. Wang, Q. Z. Shi, *Cryst. Growth Des.* 2013, **13**, 1570. (b) A. E. Platero-Prats, V. A. de la Peña-O'Shea, D. M. Proserpio, N. Snejko, E. Gutiérrez-Puebla, Á. Monge, *J. Am. Chem. Soc.* 2012, **134**, 4762. (c) N. L. Rosi, J. Kim, M. Eddaoudi, B. Chen, M. O'Keeffe, O. M. Yaghi, *J. Am. Chem. Soc.* 2005, **127**, 1504. (d) M. A. Braverman, R. L. LaDuca, *Cryst. Growth Des.* 2007, **7**, 2343. (e) W. Song, J. R. Li, P. C. Song, Y. Tao, Q. Yu, X. L. Tong, X. H. Bu, *Inorg. Chem.* 2009, **48**, 3792.

12 S. Zang, Y. Su, Y. Li, Z. Ni, H. Zhu, Q. Meng, *Inorg. Chem.* 2006, **45**, 3855.

13 (a) Q. Fang, G. Zhu, M. Xue, J. Sun, F. Sun, S. Qiu, *Inorg. Chem.* 2006, **45**, 3582. (b) S. Sanda, S. Parshamoni, A. Adhikary, S. Konar, *Cryst. Growth Des.* 2013, **13**, 5442.

14 C. A. Bauer, T. V. Timofeeva, T. B. Settersten, B. D. Patterson, V. H. Liu, B. A. Simmons, M. D. Allendorf, *J. Am. Chem. Soc.* 2007, **129**, 7136.

15 (a) Q. R. Fang, G. S. Zhu, Z. Jin, Y. Y. Ji, J. W. Ye, M. Xue, H. Yang, Y. Wang, S. L. Qiu. *Angew. Chem., Int. Ed.* 2007, **46**, 6638. (b) H. Kitagawa, Y. Ozawa, K. Toriumi. *Chem. Commun.* 2010, **46**, 6302. (c) Q. L. Zhu, C. J. Shen, C. H. Tan, T. L. Sheng, S. M. Hu, X. T

Wu. *Chem. Commun.*, 2012, **48**, 531. (d) Q. L. Zhu, T. L. Sheng, C. H. Tan, S. M. Hu, R. B. Fu, X. T Wu. *Inorg. Chem.*, 2011, **50**, 7618.

16 (a) T. Sajoto, P. I. Djurovich, A. B. Tamayo, J. Oxgaard, W. A. Goddard, M. E. Thompson, *J. Am. Chem. Soc.* 2009, **131**, 9813. (b) C. d. Tard, S. Perruchas, S. b. Maron, X. F. Le Goff, F. o. Guillen, A. Garcia, J. Vigneron, A. Etcheberry, T. Gacoin, J. P. Boilot, *Chem. Mater.* 2008, **20**, 7010.

17 (a) C. Y. Sun, X. L. Wang, X. Zhang, C. Qin, P. Li, Z. M. Su, D. X. Zhu, G. G. Shan, K. Z. Shao, H. Wu, J. Li, *Nat Commun.* 2013, **4**, 2717. (b) D. Y. Wu, W. Huang. C. Y. Duan, Z. H. Lin, Q. J. Meng, *Inorg. Chem.* 2007, **46**, 1538. (c) B. Chen, L. Wang, F. Zapata, G. Qian, E. B. Lobkovsky, *J. Am. Chem. Soc.* 2008, **130**, 6718.

18 L. Z. Zhang, W. Gu, B. Li, X. Liu, D. Z. Liao, *Inorg. Chem.* 2007, **46**, 622.

19 (a) M. A. Anderson, H. Shim, F. M. Raushel, W. W. Cleland, *J. Am. Chem. Soc.* 2001, **123**, 9246. (b) E. G. Azenha, A. C. Serra, M. Pineiro, M. M. Pereira, J. Seixas de Melo, L. G. Arnaut, S. J. Formosinho, A. M. D' A. Rocha Gonsalves, *Chem. Phys.* 2002, **280**, 177. (c) N. V. Korol'kova, V. G. Klimenko, T. A. Kir'yanova, S. A. Serov, E. A. Gastilovich, *Chem. Phys.* 1999, **248**, 233. (d) C. K. Lim, J. Shin, I. C. Kwon, S. Y. Jeong, S. Kim, *Bioconjugate Chem.* 2012, **23**, 1022. (e) M. Nag, W. S. Jenks, *J. Org. Chem.* 2004, **69**, 8177. (f) M. Rae, F. Perez-Balderas, C. Baleizão, A. Fedorov, J. A. S. Cavaleiro, A. C. Tomé, M. N. Berberan-Santos, *J. Phys. Chem. B.* 2006, **110**, 12809. (g) K. Ruud, B. Schimmelpfennig, H. Ågren, *Chem. Phys. Lett.* 1999, **310**, 215. (h) A. C. Serra, M. Pineiro, A. M. d. A. Rocha Gonsalves, M. Abrantes, M. Laranjo, A. C. Santos, M. F. Botelho, *J. Photochem. Photobiol. B.* 2008, **92**, 59. (i) I. Soutar, L. Swanson, P. G. Adamson, N. Flint, *J. Macromol.* 2009, **42**, 9153. (j) C. N. Burress, M. I. Bodine, O. Elbjeirami, J. H. Reibenspies, M. A. (k) Omary, F. P. Gabbaï, *Inorg. Chem.* 2007, **46**, 1388. (l) M. Nag, W. S. Jenks, *J. Org. Chem.* 2004, **69**, 8177. (m) M. A. Omary, R. M. Kassab, M. R. Haneline, O. Elbjeirami, F. P. Gabbaï, *Inorg. Chem.* 2003, **42**, 2176. (n) B. Wang, B. Sun, X. Wang, C. Ye, P. Ding, Z. Liang, Z. Chen, X. Tao, L. Wu, *J. Phys. Chem. C.* 2014, **118**, 1417.